

Preparation and characterization of maleated polylactide-functionalized graphite oxide nanocomposites

Yeh Wang · Chi-S. Lin

Received: 22 September 2013 / Accepted: 2 December 2013 / Published online: 11 December 2013
© Springer Science+Business Media Dordrecht 2013

Abstract Organically dispersible graphene nanosheets were fabricated by amine surfactant intercalated graphite oxide (GOAs) with ultrasonication below room temperature. Subsequently, GOAs filled nanocomposites of polylactide grafted with maleic anhydride (PLAgMA) were prepared directly by solution blending. The compatibilization effects provided by the functionalization of both constituents and their influence on the structure and properties of the final nanocomposites in different compositions were investigated. The interactions and structural morphology of the nanocomposites were examined by Fourier transform infrared spectroscopy, X-ray diffraction, scanning and transmission electron microscopy. Thermal, dynamic-mechanical and conductive properties of these nanocomposites were investigated as a function of GOAs content. The detailed morphological and X-ray diffraction results revealed that the degree of GOAs dispersion enhanced with maleated PLA. Study of the dynamic-mechanical properties showed that both the storage modulus G' and the loss modulus G'' are very sensitive to the microstructure of the nanocomposite. The thermal properties of the nanocomposites were significantly influenced by the GOAs content due to the shielding and nucleating effect of exfoliated layers. Both the thermal and electrical conductivities showed substantial improvements with increasing GOAs content. The overall results pointed to the compatibilization synergy of GO functionalization and PLA maleation.

Keywords Nanocomposite · Graphene nanosheet · Functionalization · Polylactide · Maleation

Y. Wang (✉) · C.-S. Lin
Department of Chemical and Materials Engineering, Tunghai University, Taichung, Taiwan 407, Republic of China
e-mail: yehwang@thu.edu.tw

Introduction

With ever increasing environmental concerns and fast depletion of petroleum resources, demand for alternate biodegradable plastics from renewable origin with suitable material properties is growing at a rapid rate. Biopolymers such as cellulose esters (cellulose acetate and cellulose acetate butyrate), poly(hydroxyalkanoate)s, and polylactide (PLA) are increasingly being studied as replacements for petroleum-based polymers [1–4]. The potential of these materials in medical devices, packaging, and automotive applications is continuously being explored by researchers and industry. PLA, produced through a fermenting process from annually renewable and carbon neutral resources, is a linear polyester that is biodegradable and aims to replace commodity synthetic polymers. It has an excellent balance of mechanical and rheological properties [5]; however, the inherent brittleness and low heat resistance reduce its use to very limited applications in the packaging industry [4, 6–8]. In order to overcome those drawbacks, new and enhanced grades with improved processability and end-use properties are being developed to make PLA suitable for a wider range of applications. Two recent publications [9, 10] summarized the latest development in the modification and processing of PLA. The presence of a sizable potential market for high performance engineered and durable applications may open up a significant amount of opportunities for companies within the chemical, agricultural, and plastic sectors.

The potential interest in PLA for engineering applications (electronic and electrical devices, mechanical and automotive parts, etc.) has grown rapidly, but it is required the tailoring of its properties to reach the end-user demands. For further applications, the profile of PLA properties can be tuned by combining this polyester matrix with different nanosized dispersed phases. Extensive research efforts have recently been devoted to the modification of PLA, through adding inorganic nanofillers, to enhance physical properties and/or change degradation characteristics. Though the isotropic nanoparticles such as SiO_2 ,

CaCO₃ and TiO₂ are promising for reinforcement due to their unique properties [11–15], the combination of highly anisotropic nanofillers, such as layered silicate [16–19], hydroxyapatite (HA) [20–22], POSS [23, 24], carbon nanotubes [25, 26], and graphene or graphite oxide nanosheets [27–30], with PLA showed significant improvement in properties, such as stiffness, thermal stability, fire retardancy, lower permeability, etc. Indeed, the production of filled-PLA grades using various types of nano-mineral fillers, surface-modified or not, can be an interesting solution to reduce PLA global price and to augment a wide range of performance of the PLA nanocomposites.

Furthermore, the polymer composites filled with nanosized carbonaceous fillers such as CNTs were proved to exhibit a remarkable balance of performances in terms of mechanical, fire resistance, thermal and electrical conductivities [31]. Generally, the high cost of CNTs has limited their extensive use in industrial sectors and other alternatives are to be considered. Graphite combines the lower price and the layered structure of clays with the superior thermal and electrical properties to CNTs. It can be thus an alternative to both clays and CNTs to make polymer composites with competitive multifunctional properties. Graphite consists of graphene nanosheets [32, 33], and owns thermal and electrical characteristics usually associated with metals which make it suitable for applications where its properties like heat stability, lubricant ability, thermal and electrical conductivity are required. An important number of studies have been recently carried out on dispersion of expanded graphite (EG) and exfoliated graphite nanosheets (GNS) derived from graphite oxide (GO) in engineering or commercial polymers. In all cases the acid-treated natural graphite must undergo rapid heating over 1000 °C (at a heating rate exceeding 2000 °C/min) to allow decomposition of the intercalated reactant to generate a CO₂ over-pressure and splits the graphite oxide into individual sheets typically consisting of hundreds of stacked graphite layers. However, the extreme thermal shock may result in distorted aromatic ring structures and deterioration of mechanical and conductive properties [33]. The EG or GNS reinforced/conductive polymer composites were then prepared using various techniques [34–40]: *in situ* polymerization, solution and shear mixing, melt-compounding, etc.

The alternative strategy to generate exfoliated GO would be the chemical approach, which can be performed in a suspension at mild temperatures and hence upscalability is straightforward, offers a route to large scale graphene production [41]. The plentiful oxygen-containing groups on the basal planes and edges of GO [42, 43] facilitates the uniform dispersion of GO in the aqueous media as well as in the polar polymers. However, it is very difficult for hydrophilic GO to form stable compatible systems with nonpolar polymers, which hampers the development of such polymer nanocomposites in industry. Chemical functionalization utilizing the active sites on GO could be carried out successfully [43]. For

example, several graphene derivatives modified with octadecylamine (ODA) or dodecylamine (DDA) have been reported. In these researches, several different synthetic methods, including nucleophilic substitution reaction [44, 45], amidation reaction [46, 47], phase transfer protocol [48] etc., have been adopted in order to improve the solubility of GO in organic solvents. It has been shown that synthetic routes and reaction conditions strongly influence the properties of graphite-ODA products [49]. Based on the above literature review, it is a pity that high reaction temperatures and complicated and difficult operating steps are generally needed in the aforementioned processes. Furthermore, the thermal stability of these hybrid materials was not studied.

Nonpolar polymers have been modified with the polar monomer of maleic anhydride (MA) to improve the exfoliation of organically modified layered silicates [50–53], by reason of their polar functional group that will improve the filler-matrix interactions. The results show that using MA grafted polymers as compatibilizers can improve the exfoliation in, for example, cellulose acetate [50], polypropylene [51], thermoplastic polyolefin [52], and PLA [53] nanocomposites. It has also been used in PLA/starch and PLA/poly(butylene adipate-co-butylene terephthalate) (PBAT) blends to improve the compatibility between these two pairs of immiscible phases, respectively [54, 55]. It is therefore believed that grafting MA onto PLA will help to improve the exfoliation of organically modified GO inside a PLA matrix. Although studies on PLA nanocomposites are rather abundant as aforementioned, study on the PLAGMA/graphene nanocomposites is particularly rare. To date, PLAGMA is not commercially available and there is limited literature reported on this material. Thus in the present study PLAGMA was produced through reactive melt-grafting method in the presence of dicumyl peroxide (DCP) as initiator.

In view of the success of the layered nanocomposites of maleated polylactide with organoclay [53] and the PLAGMA modified blends [54, 55], we attempted in this work to prepare the conducting nanocomposites of surfactant intercalated graphite oxide with PLAGMA via solution blending. It is hoped that this research is able to explore the potential combination of surface modification and chemical reduction of GO in producing novel nano-graphite based composites of maleated PLA. A scalable synthesis procedure of the functionalized graphene hybrids decorated with ODA by hydrogen bond is reported, which involves a sonication-assisted mixing process below room temperature and following ultracentrifugation and filtration (see Fig. 1). The modified graphene oxide nanosheets show higher dispersion in non-polar solvents and enhancement of thermal stability. The structure of the functionalized graphene was studied by Fourier transform infrared spectroscopy (FT-IR), X-ray diffraction (XRD), field-emission scanning electron microscope (FE-SEM), transmission electron microscope (TEM), thermogravimetric analyses

(TGA), etc. Moreover, the nanomaterials could be regarded as nanofillers in application for the improvement of the thermal stability of neat polymer nanocomposites. Then morphology, structures, and functional properties of PLA and PLAGMA/GOAs nanocomposites were systematically characterized and compared by adopting FE-SEM, XRD, thermal stability by TGA, thermal and mechanical properties from dynamical mechanical analysis (DMA), thermal conductivity from differential scanning calorimetry (DSC), and electric conductivity from dielectric analyzer (DEA).

Experimental

Materials PLA 4032D, supplied by NatureWorks, was composed of ca. 2 % D-lactide contents. The PLA pellets were transparent and amorphous, with T_g at 58 °C. 99 % synthetic graphite (SG, Aldrich), 90 % octadecylamine (ODA, Acros), certified 99.8 % p-xylene (Tedia), sulfuric acid synthesis grade (Scharlau, Spain), potassium permanganate reagent grade (Showa, Japan), and hydrogen peroxide reagent grade (Showa, Japan) were used as received for organically modified GO. The aqueous solutions were prepared in deionized water obtained by purification with a Sartorius Arium 611 system. 98 % maleic anhydride reagent grade (Showa, Japan), 99 % dicumyl peroxide reagent grade (DCP, Acros), were also used as received for melt-grafted PLA. HPLC grade tetrahydrofuran (THF, Tedia) was used as solvent for modifying GO and blending the nanocomposites.

Chemical oxidation of graphite The method due to Hummers and Offeman [56] was adopted to prepare graphite oxide (GO) from graphite flakes through chemical oxidation in the presence of concentrated sulfuric acid and potassium permanganate. The solid GO was separated by centrifugation, washed repeatedly with deionized water and acetone until sulphate could not be detected with $BaCl_2$ and dried overnight in an air-oven at 65 °C. The dried GO powder is mainly composed of layered, but compactly fastened nanoplatelets of graphite.

Intercalation of GO with amine surfactant Based on previous investigations [44, 57, 58], the neutral amine surfactants, ODA, was used in this study. In each case, a sample of 100 mg of GO was dispersed in 200 mL of THF in a glass beaker, followed by the addition of 400 mg of surfactants. Upon amine addition the GO solid swelled instantly. Each mixture was allowed to sonicate for 10 hs at 15 °C with a recirculating cooler using an ultrasonic processor VCX750 (Sonics & Materials), frequency 20 kHz, 750 W, equipped with a medium probe made of high grade titanium alloy. The stable dispersion of amine intercalated graphite oxide (GOA) was observed over 24 h. The GOA dispersion was subjected to high-speed centrifugation with 18000 rpm for 40 mins. The thick graphene pieces and partially

exfoliated graphite flakes settled down, and the few-layered fluffy graphene nanosheets remained in the supernatant. The code names are GOAs and GOAp for vacuum dried powders collected from supernatant and precipitate, respectively. The detailed discussions will be given later.

Synthesis of PLAGMA First, PLA, MA and DCP were physically premixed. The recipe consisted of 47.5 g PLA and 2.5 g MA. The amount of DCP was 0.25 phr based on an overall weight basis of PLA and MA. The reactive grafting process was carried out in an internal mixer (Plastograph EC, Germany) at 180 °C for 40 min. After compounding, purification process was carried out. PLAGMA was agitated in THF at 60 °C for 1 h, and the hot solution was poured into cold acetone. The precipitated polymer was washed with acetone several times, in order to remove any unreacted reagents, followed by drying in an oven at 70 °C for 24 hs. The purified PLAGMA was obtained. Molecular weight (MW) and molecular weight distribution (MWD) were determined using a conventional calibration size exclusion chromatography (SEC, Shimadzu LC-20AT) operating in THF at 25 °C. The method employed a single concentration detector, a refractive index (RI), to determine the concentration of the solution as it elutes from the SEC column. The calibration for molecular weight analysis is made with a series of standard narrow-distribution linear polystyrene. Then it measured the retention volume (RV) of the resulting peak apex. Finally a calibration curve of $\log(MW)$ vs $\log(RV)$ is constructed. A computer software is used for fitting the calibration curve and calculating the average molecular weight of the unknown sample. The determined number average molecular weight M_n of PLAGMA was 67,000, and the polydispersity PDI was 1.25.

Degree of grafting determination Degree of grafting (DG) for PLAGMA was determined through titration. 1 g of purified PLAGMA was refluxed in 100 mL of THF for 1 h. It was then titrated immediately with 0.005 M potassium hydroxide (KOH) using phenolphthalein as indicator. The DG can be calculated by Eq. (1):

$$DG(\%) = \frac{N \times (V_1 - V_0) \times 98.06}{2 \times W \times 1000} \times 100\% \quad (1)$$

where N is the KOH concentration [M], W is the sample weight [g], V_0 and V_1 is the KOH volume [mL] for blank solution and for titration of PLAGMA, respectively. The calculated DG of PLAGMA was 0.63.

Solution-blended PLAGMA/GOAs nanocomposites Appropriate amount of PLAGMA were completely dissolved in THF in a 250 ml glass beaker at room temperature, and subsequently the GOAs suspension was added dropwise. After sonicated

for 3 hs, a significant portion of THF was evaporated in a fume hood. Finally, the concentrate was vacuum dried at 70 °C for 48 hs. The resulting loose powder was hot pressed to produce the testing specimens. The composition of each PLA nanocomposite was confirmed by thermal gravimetric analysis based on the graphite content in the range of 1 to 5 wt.%.

Characterization Wide-angle X-ray diffraction (WAXD) patterns of different samples were recorded on a Shimadzu XRD-6000 (40 kV/40 mA) diffractometer using Cu K α radiation to characterize the nano-graphite dispersion and the crystalline structure of PLAGMA. Infrared spectra were recorded on a Shimadzu FT-IR spectrometer (Prestige-21) to identify the chemical groups of graphite due to oxidation and intercalation. The samples were measured in the form of KBr pellets. SEM images of the morphology of GO and GOS powders were observed by field-emission scanning electron microscope (FESEM) JSM-6400 (JEOL, Japan) with accelerating voltage of 12 kV and working distance of 15 mm. The dispersion of graphite particles within the PLAGMA matrix was also studied by SEM. The freeze-fractured sample surfaces were metallized with platinum using an ion coater IB-3 (Giko, Japan). Transmission electron microscopy (TEM) JEM-1200EX (JEOL, Japan) was used for direct observation of the intercalated lamellar structure of graphite oxide in the nanocomposites. Ultrathin samples were obtained by microtoming the sample plates.

The nonisothermal degradation behavior of PLAGMA and its composites with GOAs was characterized by using a

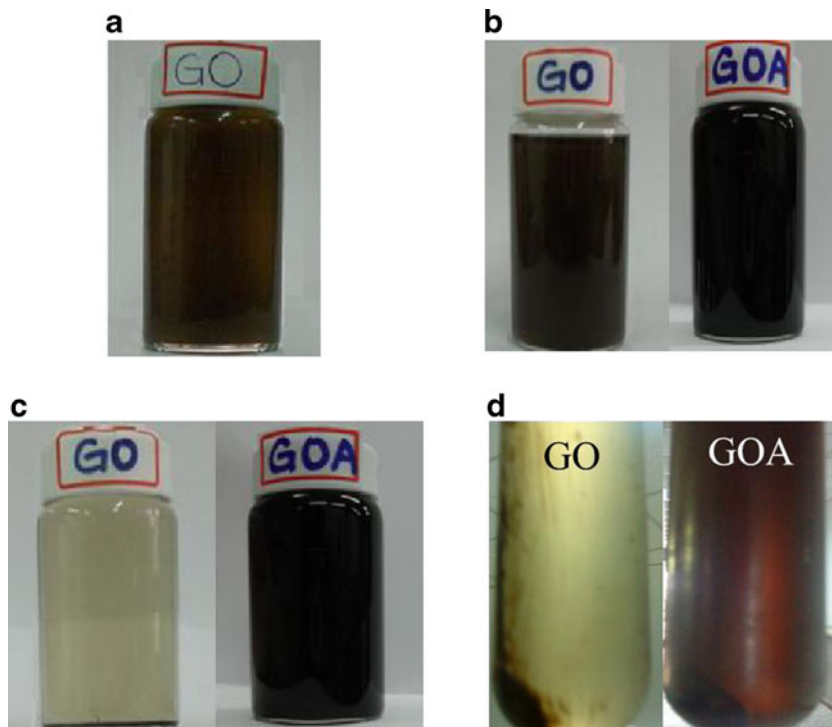
thermogravimetric analyzer (TGA Q500, TA Instrument). All measurements were performed under a nitrogen atmosphere from room temperature to 800 °C at a heating rate of 20 °C min⁻¹. Thermal properties of the composites were characterized using a Perkin-Elmer DSC Pyris 1 (Perkin Elmer, Boston, MA). Thermal conductivity measurements were performed on the same DSC following the previous procedures [59]. Dynamic mechanical analyzer (DMA), Perkin-Elmer 7e, was used to assess the mechanical performance of the composites. For the dielectric measurements of the neat PLAGMA and the nanocomposites covering the temperature range from 30 to 130 °C and the frequency range from 10⁻² to 10⁴ Hz were carried out with a TA high-performance dielectric spectrometer DEA 2970.

Results and discussion

Structural evolution of GO (graphite oxide) and GOA (amine surfactant intercalated GO)

Preliminary characterization of the filler was carried out. To directly observe the synthetic results, the distinct solubility of GO and GO-alkylamine nanomaterials in THF have been shown in Fig. 1. Approximately 100 mg of GO powder was added to a given volume of solvent (ca. 200 ml), in such a way that the resulting nominal concentration was adjusted to 0.5 mg ml⁻¹ for all cases. The photographs showing the

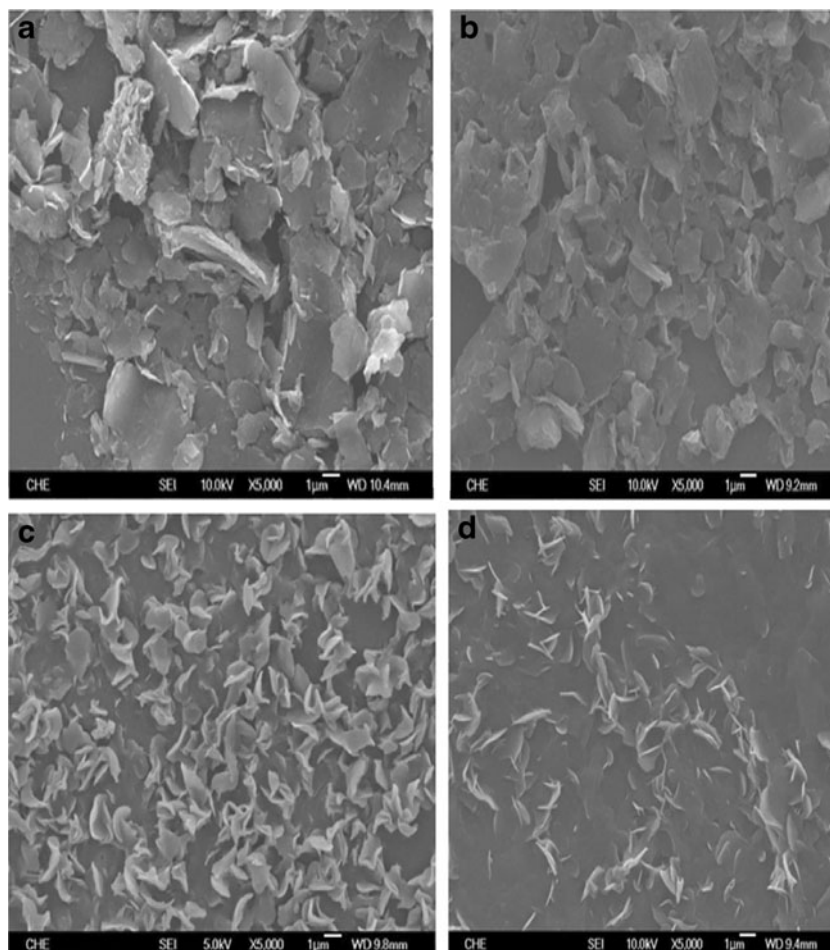
Fig. 1 Photographs of GO before sonication (a), GO and GOA after sonication for 10 hs (b), GO and GOA settled for 12 hs (c), and GO and GOA after centrifugation for 40 mins (d) in THF



original GO (dark brown, Fig. 1a); GO and GO with amine surfactant after sonication for 10 h (both fully dark, Fig. 1b); GO and GOA settled for 12 hs (GO almost settled out, but GOA suspension still stable, Fig. 1c); and GO and GOA after centrifugation (nearly transparent supernatant for GO, and opaque supernatant for GOA, Fig. 1d). Comparing Fig. 1a with 1b, it can clearly be seen that the color change from dark brown to fully dark after sonication indicated the simultaneous production of functionalized and reduced GO (also refer to the discussion of FT-IR spectroscopy at later section). At this stage, both samples formed homogeneous suspension in THF. However, as seen from Fig. 1c after settling for 12 hs, GO almost settled out with transparent supernatant, but GOA suspension remained stable. Finally, after high-speed centrifugation, the GO suspension separated into nearly transparent supernatant and dark precipitate. On the other hand, though the GOA suspension showed the dark precipitate, its supernatant became opaque with brownish color. As expected, the amine surfactant effectively modified the surface characteristics of GO. The presence of the long alkyl chains not only makes GO more hydrophobic, but helps to exfoliate the GO flakes into nanosheets, which were able to suspend in the supernatant even after centrifugation.

The structure of the filler was further investigated under a scanning electron microscope, shown in Fig. 2(a–d) for the graphite flakes of SG, GO, GOAp, and GOAs, respectively, after the sonicated dispersion dried on a glass for 24 hs. The starting material is the pristine synthetic flake graphite (SG) in the form of large thick plates as shown in Fig. 2a. The arithmetic means of the particle dimensions were obtained by averaging at least 20 particles from the micrographs taken at different regions of the same specimen. Note that the GO flake (Fig. 1b), with the thickness less than 0.2 μm , is apparently thinner than that of SG due to oxidative intercalation. Furthermore, the intercalating effect of amine surfactants can be clearly seen in Fig. 2c and d, where the stack of graphite flakes were exfoliated into thin plates, whose average thickness was around 60 nm for GOAp and 30 nm for GOAs, both generally thinner than that of GO. It can also be seen from the two figures that most GOA nanoplates were fragmented under prolonged oxidation and ultrasonication [60, 61], and produced nanosheets with diameters ranging from about 1 to 10 μm . These thin plates, not able to sustain large deformation under ultrasonication, were also corrugated with a wrinkled-paper like structure.

Fig. 2 SEM micrographs of a SG; b GO; c GOAp; and d GOAs (x5000)



The powder X-ray diffraction (pXRD) patterns of GO, the as prepared alkylamine intercalated GOAp and GOAs, are compared with that of the neat SG in Fig. 3. As expected, SG has a prominent, characteristic peak at $2\theta=26.2^\circ$, corresponding to an inter-graphene sheet spacing of 0.34 nm. However, the diffraction peak of GO shifted to the left of SG due to the effect of oxidative intercalation. The interlayer spacing was increased to 0.77 nm in GO. Further, compared to the parent GO, in the ODA intercalated samples the diffraction peak shifted further to the left. There is an apparent increase of the d_{001} value up to 2.85 and 3.15 nm for GOAp and GOAs, respectively. The increased value confirms the incorporation of the ODA molecules in the interlayer space of GO. The amine molecules could be inserted in the interlayer zone of GO either by hydrogen bonding interactions between amine molecules and oxygen containing functional groups of GO or by exchange of protons of the acidic groups of GO with alkylamines or due to amine nucleophilic attack on the epoxy groups of GO [46].

To further confirm their structural features and the existence of interactions, FT-IR spectra of GO and the corresponding derivatives were recorded in Fig. 4. The spectrum of GO is in good agreement with previous works [57, 58]. The broad band at 3416 cm^{-1} is attributed to stretching of the O–H bond of C–OH or water. The band at 1724 cm^{-1} is associated with stretching of the C=O bond of carbonyl or carboxyl groups. The band present at 1618 cm^{-1} is attributed to deformations of the O–H bending vibrations, or skeletal ring vibrations of graphitic domains [62]. Stretching vibrations of the C–O–C bond is observed as the intense band present at 1051 cm^{-1} . After functionalization, the band of GO at 1724 cm^{-1} disappears and a new band around 1580 cm^{-1} , assigned to the carboxylic acid salt (COO^-) asymmetric stretch mode, is observed. Also, the new bands due to $-\text{CH}_2$ at 2920 , 2848 and 720 cm^{-1} group together with the peak at 1466 cm^{-1} (C–N stretch of amide) [46] in the spectrum of GO-alkylamine, strongly supporting the existence of the alkyl

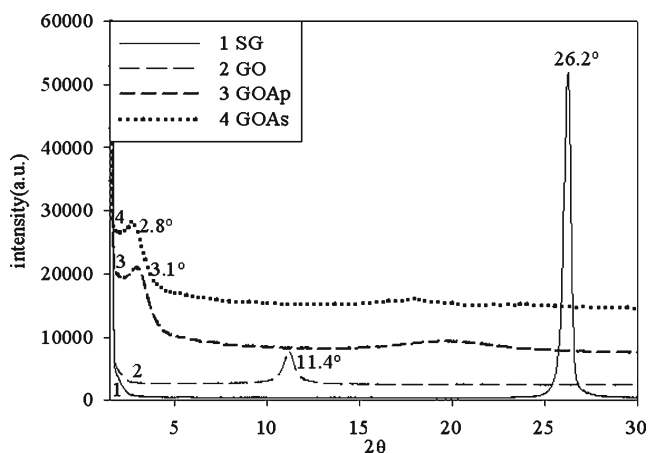


Fig. 3 WAXD patterns of a SG; b GO; c GOAp; and d GOAs

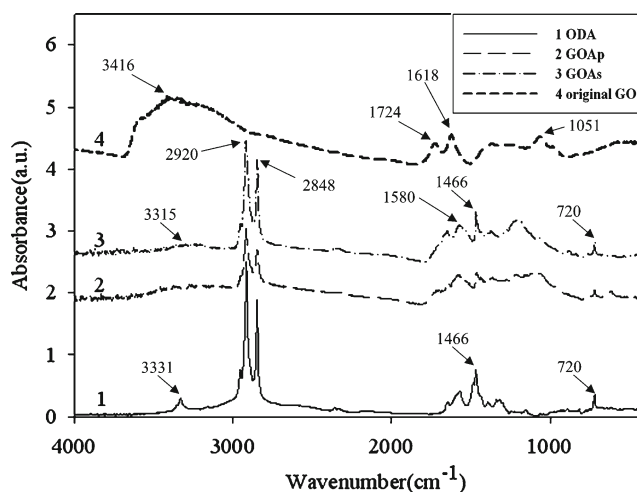


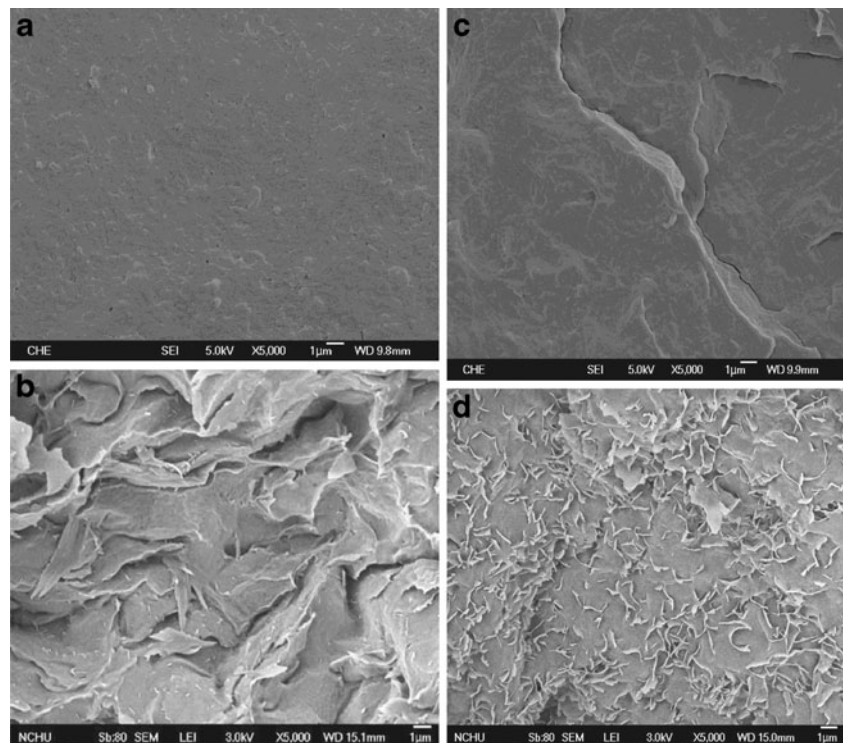
Fig. 4 FTIR spectra of ODA, GO, GOAp and GOAs

chain on GO derivatives [45]. In short, absorbances in the FT-IR spectrum attributable to the O–H, C–OH and epoxide groups in the starting material were attenuated or completely disappeared, which clearly demonstrated the reduction of GO under long-period ultrasonication. Moreover, the absorbances associated with methylene and amine groups showed the effectiveness of amine intercalation of GO.

Morphology of PLAGMA/GOAs nanocomposites

We now investigate the morphology and properties of the nanocomposites. Figure 5a–d are the images of the cryogenically fractured surfaces of pure matrices and PLA and PLAGMA/GOAs nanocomposites at 5 wt.% loading, respectively, at a magnification of $\times 5000$. PLA (Fig. 5a) and PLAGMA (Fig. 5c) homopolymers shows a very clean and smooth fractured surface due to the brittle failure behavior at room temperature. As can be seen from Fig. 5b and d, the images of the stacked graphite flakes or nanoplatelets appear brighter in contrast to the surrounding matrix, and most of the nanofillers are embedded in the polymer matrix. The thin platelets could either bend/buckle or agglomerate in response to the shear condition they experienced in the sonication bath during solution blending. Indeed the edge-on view of the nanofillers seen on the fractured surfaces showed that they could be well exfoliated in the composites with a thickness less than 100 nm with ultrasonication processing congruent with observations in Fig. 2c and d. However, close examination of the two figures reveals an extraordinary difference in the interfacial interaction between the polymer matrix and the nanofiller. It is noticeable that the buckled thin plates of GOAs and PLA matrix forming phase-separated microstructures (Fig. 5b). The formation of microcavities at the filler-matrix interface is caused by the poor compatibility between PLA and GOAs. The cracks along the PLA/GOAs interface indicated that the interfacial debonding is predominant between

Fig. 5 SEM micrographs of the cryogenically fractured surfaces **a** neat PLA; **b** PLA/GOAs; **c** neat PLAGMA; and **d** PLAGMA/GOAs (5 wt.%) at x5000



GOAs and PLA matrix, whereas a stronger bond with the PLAGMA matrix is evident such that there is no clear filler delamination from the matrix (Fig. 5d). Though most exfoliated nanofillers were embedded in the PLA matrix, some thin plates were stacked together near the cracks or defects indicated by the dark areas on the fractured surface, and they also protruded cleanly from the surface implying a weak interfacial bond. The high degree of agglomeration is attributable to the weak interfacial adhesion between GOAs and PLA matrix, and hence more susceptible to agglomerate during processing resulting in loss of its platelet morphology within the polymer matrix. It is reasonable to suppose that partial hydrolysis occurred in the anhydride functional groups interacting with the alkylamine and the hydroxyl or epoxide groups remained on GOAs surface by forming hydrogen bonds, similar to the PPgMA modified PP/LDH hybrids [63], resulting in enhanced interfacial adhesion between the nanofiller and PLAGMA.

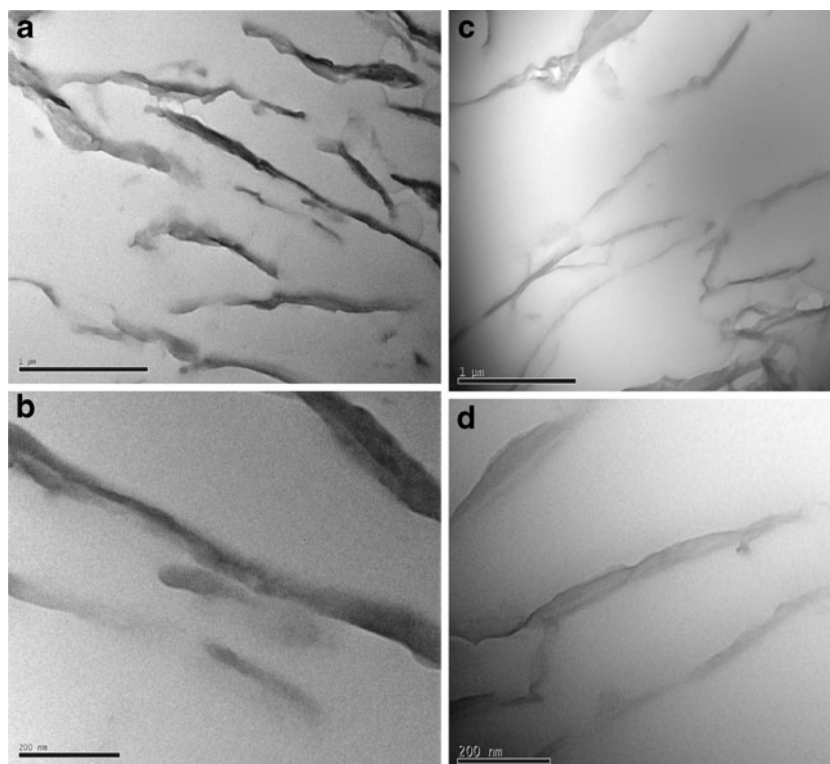
Figure 6a–d show the repeatable and representative TEM micrographs of the PLA and PLAGMA/GOAs composites with two magnifications, respectively. As shown in both figures, the original graphite stacks of GOAs were partially exfoliated into a thinner multilayered structure or even nanolayers. As a result, no discernable diffraction peak was shown in the corresponding XRD patterns (see Fig. 7). The dark or gray sections and the bright domains are referred to as the intercalated graphite sheets and the polymer matrix, respectively. Further, the dark stripes representative of the aggregated graphite layers of GOAs in PLA (Fig. 6a and b) are

clearly thicker than that in PLAGMA (Fig. 6c and d). As for the PLAGMA nanocomposites, it can be seen that there exist a group or several groups of parallel graphite sheets (shown as thin gray lines) with a thickness of 30 nm approximately and a gallery of intercalated stacks (shown as expanded gray stripes) about 90 nm on average, finely dispersed in the PLAGMA matrix, which is in good agreement with the previous literatures about PLA/EG or GO nanocomposites prepared via melt or solution blending method [28, 64]. This demonstrates the effect of amine surfactant intercalation, leading to the significant improvement of the interfacial adhesion between GOAs and PLAGMA matrix.

Wide angle X-ray diffraction

XRD was also employed to further characterize graphite dispersion in the PLAGMA composites. We only showed the X-ray diffractograms of unfilled PLAGMA and its composites with graphite loading of 1, 3 and 5 wt.% in Fig. 7 for the reason of clarity. In nanocomposites containing organoclay, increasing exfoliation is associated with a reduction of the peak intensity in XRD characteristic of the repeated layer spacing. We apply this same principle in graphite-based samples. While the pristine SG exhibits a diffraction peak at 26.6° , it is obvious that the peak associated with the inter-graphene sheet spacing is almost totally suppressed in the PLAGMA/GOAs specimens. This strongly suggests that significant exfoliation/dispersion of the GOAs flakes was achieved under ultrasonication. The X-ray diffraction results supplement the

Fig. 6 TEM micrographs of the nanocomposites at 5 wt.% loading. **a** PLA/GOAs and **b** PLAGMA/GOAs at $\times 120000$



morphological observations from electronic microscopy. Furthermore, as seen in Fig. 7, the X-ray diffractogram of neat PLAGMA (solid line) has several peaks between $2\theta = 14.7^\circ$ and 22.5° , consistent with the PLA crystal unit cell [26, 27]. The similar diffraction patterns observed between PLAGMA and the nanocomposites, indicating that the incorporation of GOAs does not modify the crystal structure of PLA in the nanocomposites. In addition, the strongest diffraction peaks appearing at 16.7° and 19.1° represent (200)/(110) and (203) reflections of stable α -form crystal. The two peak intensities

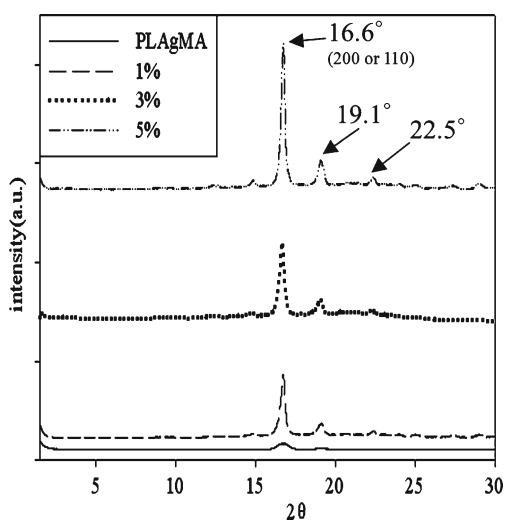


Fig. 7 WAXD patterns of neat PLAGMA and composites with various graphite loadings

were considerably more intense for PLAGMA composites than the unfilled PLAGMA. It has been reported [26] that the high intensity at 16.7° in the presence of GOAs was attributed to the strong preferential growth of PLA crystallites largely along the a-axis during nucleation, since the dominant diffraction peak corresponds to (200) reflection of α -form of crystalline PLA. Note that all the specimens were prepared from compression molding. The low crystalline reflection intensities of neat PLAGMA demonstrate its inherent low crystallization rates. The PLAGMA/GOAs systems exhibit peaks associated with neat PLAGMA, and the peak intensities of the two strongest peaks increase with GOAs loading in the hybrids. The nucleating effect of GOAs on PLAGMA matrix will be further investigated in the crystallization and melting behavior of the composites using DSC.

Thermal stability of PLAGMA/GOAs nanocomposites

Figure 8 shows TGA thermograms (Fig. 8a) and their derivative weight curves (Fig. 8b). Again only the measurements of PLAGMA/GOAs composites with 1, 3, and 5 wt.% graphite contents were presented for the reason of clarity. Thermal degradation profiles of the nanocomposites displayed that thermal stability of the nanocomposites was improved with the increasing GOAs content. For the quantitative comparison of thermal stabilities among the tested specimens, the maximum thermal degradation temperatures, T_d , evaluated from the peak value of DTG curves were summarized in Table 1,

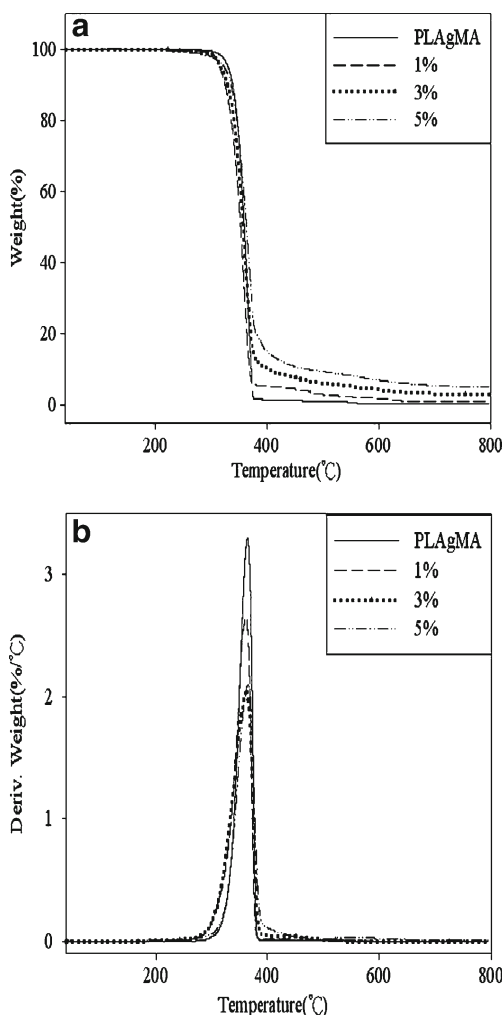


Fig. 8 a TG and b DTG curves of neat PLAGMA and its composites with various graphite loadings at a heating rate of 20 °Cmin⁻¹

together with the weight fractions of graphite and PLAGMA matrix of each composite. Note that the weight fractions of amine content and hence the polymer content were determined from the TGA results of the GOA powders, and the graphite contents were confirmed by the residual weights in Fig. 8a. It can be seen clearly in this figure that the graphite residuals of the composites increased with increasing graphite content. However, as listed in Table 1, the PLAGMA content decreased

Table 1 Degradation temperatures and thermal properties of PLAGMA and PLAGMA nanocomposites with graphite loading in the range from 1 to 5 wt.%

Sample	T _d (°C)	T _g (°C) (from cooling)	T _m (°C)	ΔH _m (J/g)	T _c (°C)	ΔH _c (J/g)
Neat PLAGMA	355.4	56.2	171.58	26.78	98.0	–
Composite composition graphite matrix						
1 %	96.0 %	360.8	56.0	169.58	37.50	100.3
2 %	91.6 %	361.2	56.6	169.49	39.8	101.4
3 %	87.8 %	362.3	56.9	169.23	42.5	105.3
4 %	83.8 %	363.2	58.1	169.56	48.8	106.2
5 %	80.0 %	364.8	58.8	169.56	52.9	106.6

from 96 to 80 wt.% as the graphite content increased from 1 to 5 wt.% with increasing dose of amine surfactant.

Next, the T_d of unfilled matrix PLAGMA was determined to be about 355.4 °C. Indeed, the T_ds of the composite of the lowest graphite content (1 wt.%) increased ca. 5 °C, and the increase for the highest content (5 wt.%) was ca. 10 °C higher than that of the neat matrix. This improved thermal stability of the nanocomposites is believed to originate from the fact that graphite nanoplatelets of GOAs, which were dispersed homogeneously in the PLAGMA matrix, serve as the mass transfer barriers against the volatile pyrolyzed products in the PLAGMA matrix, eventually retarding thermal degradation of the nanocomposites. Finally, we also noticed that the onset of thermal decomposition was earlier for the nanocomposites compared to pure PLAGMA. The free surfactant and other small molecule impurities may cause the nanocomposites decompose earlier than the pure PLAGMA. However, after decomposition of the volatile components, the functionalized graphene nanosheets played the major role in increasing the maximum degradation temperature of the nanocomposites.

DSC and thermal conductivity measurements

Figure 9 shows the DSC heating (9a) and cooling (9b) curves of neat PLAGMA and the PLAGMA composites. In Table 1 we summarized the values of the temperature and the enthalpy of melting and crystallization. The values of ΔH_m and ΔH_c were normalized by the weight content of PLAGMA in the composite. We first take a look at the melting peak temperatures (Fig. 9a), T_m, in Table 1. The T_ms of all the composites were nearly the same at 169.6 °C, about 2 °C less than that of neat PLAGMA. This can be explained on the basis of heterogeneous and homogeneous nucleation of PLAGMA. It has been reported [64] that the addition of graphene promoted the heterogeneous nucleation resulting in a large number of small spherulites in the hybrid in comparison with the homogeneous nucleation of neat PLA. The presence of graphene may induce some defects or disordered microstructures in the spherulitic morphology, resulting in lower T_m, by acting as nucleating agent, but the crystalline structure, as shown in the X-ray diffractograms in Fig. 7, remained the same. On the other hand, the crystallization peak temperatures (Fig. 9b), T_c, of

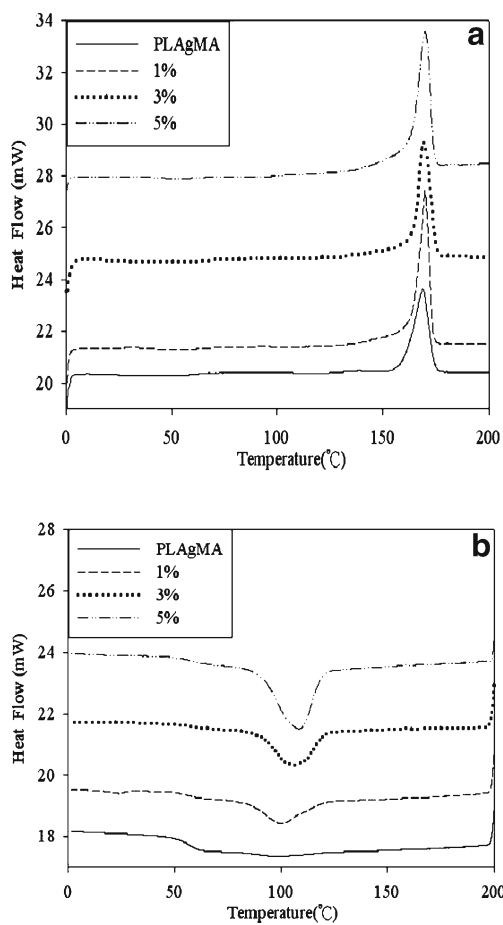


Fig. 9 DSC thermograms of PLAGMA and nanocomposites **a** heating traces, and **b** cooling traces with various graphite loadings

the composites vary from 98 °C for unfilled specimen to 106.6 °C for 5 wt.% composite. Apparently, T_c increased from 2 to 8 °C with GOAs loading varying from 1 to 5 wt.% relative to neat PLAGMA. This was due to the nucleating effect of GOAs on PLAGMA crystallization. Accordingly, the normalized degree of crystallinity (ΔH_c and ΔH_m) of PLAGMA in the composites is also increasing with GOAs loading, but the unfilled PLAGMA showed no crystallization peak. The DSC results are consistent with X-ray diffraction measurements. They both point to the apparent effect of nucleation, which could be probably attributed to the enhanced interfacial interaction between PLAGMA and GOAs resulting from the great increase in the specific surface area of GOAs after exfoliation/dispersion in the sonication bath.

The thermal conductivity reported is the average value of three samples cut from different specimens. The melting curves of pure gallium (m.p. at 29.8 °C) with different samples are shown in Fig. 10(a) and (b) for PLA and PLAGMA nanocomposites, respectively. Note that the gallium-DSC method used here is limited to the through-plane conductivity [59]. As expected, the start-up temperatures of the melting of gallium with both nanocomposite shifted to lower

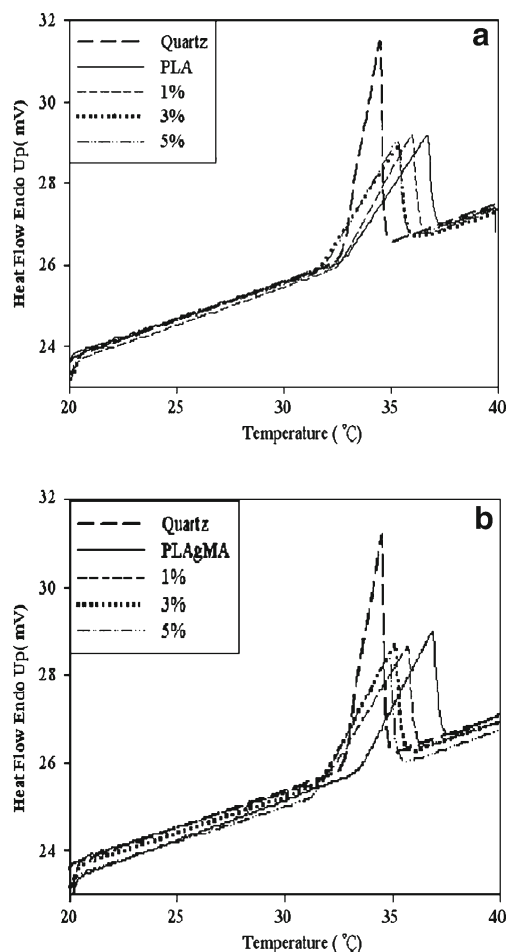


Fig. 10 DSC melting curves of gallium with variations in thermal conductivities of **a** PLA and **b** PLAGMA and composites with various graphite loadings

temperatures than the unfilled matrices. Further, the GOAs filled samples yielded the melting curves with slopes increasing with GOAs loading. For both composites, the steepest slope at 5 wt.% corresponding to the highest thermal conductivity is nearly double that of neat resin. The improvement is mainly due to effective dispersion of GOAs in the matrix, giving rise to the high aspect ratio of the graphite nanosheets and hence a smaller contribution from thermal contact resistance. In addition, the thermal conductivities for PLAGMA nanocomposites, varying from 0.22 to 0.36 W/m °C with 1 to 5 % GOAs, were all higher than their PLA counterparts, which were in the range of 0.18–0.29 W/m °C. The better improvement in thermal conductivity demonstrated the higher degree of dispersion and exfoliation of GOAs in PLAGMA filled hybrids than in PLA ones consistent with the observed morphology (see Figs. 5 and 6). Since only the through-plane conductivities were measured here, they were much lower than the in-plane thermal conductivity of graphite which is 210–230 W/m °C. Also recall that the morphological examination of the composites indicated that these large platelets

were not perfectly well-dispersed and showed evidence of agglomeration as indicated in SEM micrographs. Additionally, the graphite sheets were not planar but were buckled or rolled-up into cylinders as shown in those figures, which reduced the aspect ratio and changed the assumed platelet geometry resulting in much lower thermal conductivity in the composites than the pure graphite. Finally it should be noted that the method used, i.e., using the slope of a heat flux vs. temperature plot obtained by DSC of the gallium-composite sample, becomes less sensitive at higher thermal conductivities. In any case, the method is sufficient for screening experiments of low filler contents with thermal conductivity lower than 1.2–1.5 W/m °C.

Dynamic mechanical analysis

The dynamic mechanical behavior of neat PLAGMA and PLAGMA/graphite nanocomposites are presented in Fig. 11 with graphite loading from 1 to 5 wt.%. The storage (or

elastic) moduli (E') are presented in Fig. 11a. The E' values of all the specimens at nominated temperatures are listed in Table 2. From the E' curves it is apparent that, in the presence of graphite fillers, the E' of the composites was greater than that of unfilled PLAGMA throughout the test temperature range. The magnitudes of E' again increase with increasing graphite loading, where the relative increase was ca. 10 % for 1 wt.% loading to 20 % for 5 wt.% loading higher than the unfilled matrix.

The significant increase of E' of filled PLAGMA is believed attributed to the effective exfoliation/dispersion of GOAs (as a result of interaction between GOAs and MA functional group). This overabundance of graphite nanosheets results in enormous increase in the surface area available for bonding to MA substituents. The glass transition (T_g), which is the viscoelastic transition of a material, is often drawn from the maxima of E'' curve as shown in Fig. 11b. In this case the peak values in the E'' curves were used to obtain T_g . The T_g of the unfilled PLAGMA is approximately 64.3 °C. It can be clearly seen that the T_g 's of the nanocomposites are all higher than that of unfilled PLAGMA, where the increase was ca. 10 % for 5 wt.% composite. The increase in T_g is ascribed to a decrease in mobility of the polymer chains, due to the strong interactions of hydrogen bonding between the polar groups of PLAGMA and GOAs. The same observation has been reported in the dynamic mechanical behaviors of other filled polymeric systems [65]. Note that We would emphasize here that the changing trends of T_g , which increases with increasing graphene content in the nanocomposites, are qualitatively consistent from either DSC or DMA despite the differences in the T_g values from both measurements (see Tables 1 and 2).

Electrical properties of PLA/GOAs nanocomposites

Figure 12(a) and (b) show the changes of the ac conductivities at 50 °C of PLA and PLAGMA/GOAs composites as a function of frequency with the graphite content varying from 1 to

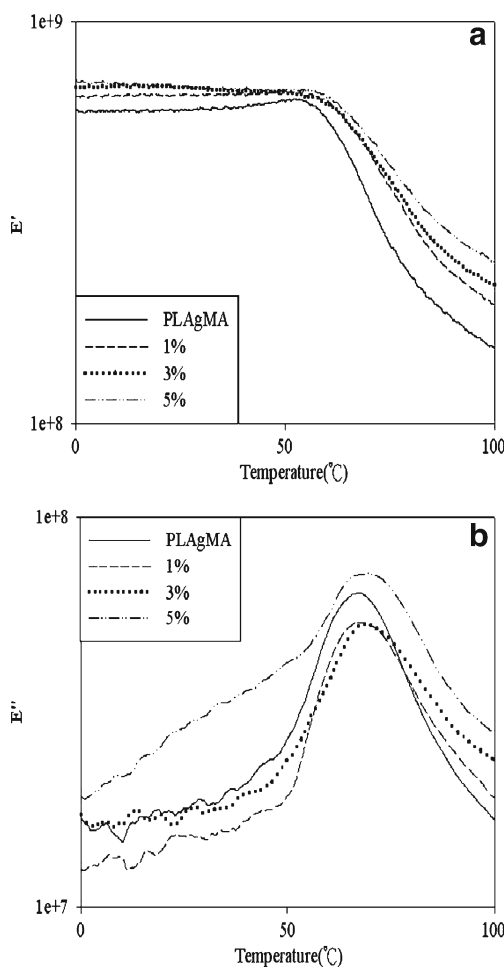


Fig. 11 Dynamic mechanical spectra **a** storage modulus E' ; and **b** loss modulus E'' for neat PLAGMA and composites with various graphite loadings as a function of temperature

Table 2 Dynamic storage moduli and glass transition temperatures of unfilled PLAGMA and PLAGMA nanocomposites at nominal temperatures

	T_g (°C)	E' (MPa)		
		-20 °C	30 °C	80 °C
neat PLAGMA	64.3	607.0	611.3	232.6
1 %	65.1	639.4	662.0	319.0
2 %	65.6	675.3	676.4	312.1
3 %	68.6	699.6	687.6	336.4
4 %	69.6	717.9	689.7	354.7
5 %	69.7	733.3	688.7	375.9

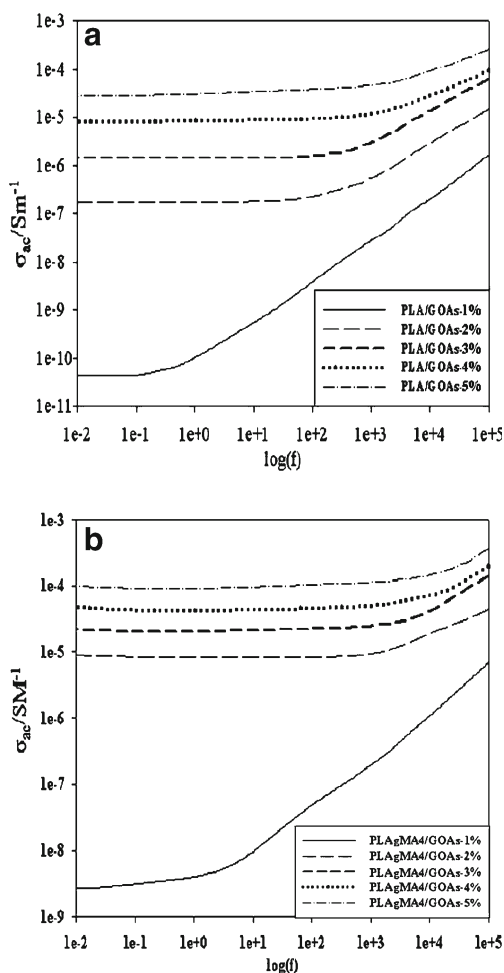


Fig. 12 Ionic conductivity of **a** PLA and **b** PLAGMA/GOAs nanocomposites as a function of frequency at 50 °C with graphite loadings from 1 to 5 wt. %

5 wt.%. Note that the ac conductivity was calculated from dielectric loss with the following equation [66]:

$$s_{ac} = \omega \epsilon_0 \epsilon'' \quad (2)$$

where ω is the angular frequency, ϵ_0 is the absolute permittivity of free space, and ϵ'' is the dielectric loss. It is clearly seen that σ_{ac} changes drastically with frequency. At low frequency a plateau where σ_{ac} is frequency independent can be observed clearly in the plots. At higher frequencies, σ_{ac} increases rapidly with increasing frequency. The transition region from dc (frequency-independent ionic conductivity) to ac (frequency-dependent) conductivity shifts to higher frequencies with increasing graphite content. Note that the ionic conductivity of neat PLAGMA is evaluated to be in the order of 10^{-13} Sm^{-1} , which is not shown here. Furthermore, for both nanocomposite, it is apparent that the ionic conductivities exhibit a sudden increase at the filler content beyond around 1 wt.%, at which the percolation threshold of electrical

conduction path for graphite nanoplatelets of GOAs was achieved in the PLA and PLAGMA matrices. We believe that the relatively low graphite content of electrical percolation threshold for both hybrids is associated with the homogeneous dispersion of GOAs in the polymer matrix. Furthermore, the ionic conductivities of the PLA/GOAs composites changed from 10^{-11} to 10^{-5} Sm^{-1} with 1–5 % graphite content, however, the ionic conductivity of PLAGMA hybrids was in the range of 10^{-9} to 10^{-4} Sm^{-1} . It is apparent that the greater degree of exfoliation/dispersion of GOAs in the PLAGMA matrix also gave rise to the higher ionic conductivity than the PLA composites at all graphite levels. It is noticeable that the ionic conductivity of 10^{-4} Sm^{-1} of PLAGMA/GOAs nanocomposites is low enough to attain the electrostatic dissipation and/or partial electromagnetic dissipation for thermoplastics, fibers, and films.

Conclusion

The addition of amine surfactant was found to significantly affect the layered structure and enhance the degree of exfoliation/dispersion of GOAs (i.e. the amine-surfactant intercalated GO). As evidenced by XRD, GO was well intercalated, and the diffraction peaks of the inter-graphene sheet spacing shifted to lower angles after intercalation by ODA. The electron microscopic studies clearly showed that the thickness of GOAs flakes has been reduced significantly compared to that of GO with ultrasonication. Additionally, the WAXD analysis of PLAGMA/GOAs composites exhibited α crystalline peaks, however, the peak intensity were greater than that of unfilled PLAGMA. The results were consistent with the DSC analysis, where the normalized melting enthalpies of the composites were also greater than the neat resin.

Both the thermal conductivity and the dc ionic conductivity were significantly increased in the PLAGMA/GOAs composites. Note that degree of exfoliation, orientation, and interfacial interaction have an influence on the conductive properties in composites. The interfacial interactions between PLAGMA and GOAs were improved by the organic intercalant. However, unlike the exponential increase in ionic conductivity, thermal conductivity enhancement by GOAs is not as dramatic [63]. This is partly due to smaller contrast in thermal conductivity between polymers and graphitic carbons than that in electrical conductivity. The dynamic mechanical properties indicated that GOAs had a reinforcing effect on the elastic behavior of PLAGMA. The composite materials exhibited increasing G' and T_g with GOAs content. This was thought to be due to the ease of PLAGMA diffusing into the gallery of GOAs. The confined polymer chains in the gallery were not free from chain motion through the hydrogen bonding of polar groups in the individual constituents. The superior properties of PLAGMA/GOAs system reflect the compatibility between

the GOAs nanosheets and the PLAGMA matrix. Furthermore, the improvement in both the thermal and electrical properties can be further optimized by enhancing the compatibility and adhesion at the PLAGMA-GOAs interface, and by improving the dispersion and orientation of the graphite nanosheets by selecting long chain surfactant. Overall, chemically exfoliated nanosheets plus functionalized polymers have demonstrated an exciting new ability to simultaneously improve multiple physical, thermal and mechanical properties of polymer composites making GOAs a multifunctional nano-reinforcement.

Acknowledgments The financial support of this research by the NSC of Taiwan under the grant NSC-101-2221-E-029-002 is gratefully acknowledged.

References

- Ak M, Wibowo A, Misra M, Drzal LT (2004) Effect of process engineering on the performance of natural fiber reinforced cellulose acetate biocomposites. *Compos A* 35:363–370
- Petersen K, Nielsen PV, Olsen MB (2001) Physical and mechanical properties of biobased materials starch, polylactate and polyhydroxybutyrate. *Starch* 53:356–361
- Bastioli C (2001) Global status of the production of biobased packaging materials. *Starch* 53:351–355
- Lunt J (1998) Large-scale production, properties and commercial applications of polylactic acid polymers. *Polym Degrad Stab* 59: 145–152
- Vert M, Schwarch G, Coudane J (1995) Present and future of PLA polymers. *J Macromol Sci Part A* 32:787–796
- Labrecque LV, Kumar RA, Dave V, Gross RA, McCarthy SP (1997) Citrate esters as plasticizers for poly(lactic acid). *J Appl Polym Sci* 66:1507–1513
- Martin O, Averous L (2001) Poly(lactic acid): plasticization and properties of biodegradable multiphase systems. *Polymer* 42:6209–6219
- Jacobsen S, Fritz HG (1999) Plasticizing polylactide—the effect of different plasticizers on the mechanical properties. *Polym Eng Sci* 39: 1303–1310
- Auras RA, Lim LT, Selke SEM, Tsuji H (eds) (2010) Poly(lactic acid): synthesis, structures, properties, processing, and applications. Wiley, NJ
- Ren J (ed) (2011) Biodegradable poly (lactic acid): synthesis, modification, processing and applications. Springer, Heidelberg
- Jiang L, Zhang JW, Wolcott MP (2007) Comparison of polylactide/nano-sized calcium carbonate and polylactide/montmorillonite composites: reinforcing effects and toughening mechanisms. *Polymer* 48: 7632–7644
- Yan SF, Yin JB, Yang Y, Dai ZZ, Ma J, Chen XS (2007) Surface-grafted silica linked with L-lactic acid oligomer: a novel nanofiller to improve the performance of biodegradable poly(L-lactide). *Polymer* 48:1688–1694
- Nakayama N, Hayashi T (2007) Preparation and characterization of poly(L-lactic acid)/TiO₂ nanoparticle nanocomposite films with high transparency and efficient photodegradability. *Polym Degrad Stab* 92:1255–1264
- Fukuda N, Tsuji H (2005) Physical properties and enzymatic hydrolysis of poly(L-lactide)-TiO₂ composites. *J Appl Polym Sci* 96:190–199
- Wei J, Chen QZ, Stevens MM, Roether JA, Boccaccini AR (2008) Biocompatibility and bioactivity of PDLA/TiO₂ and PDLA/TiO₂/Bioglass® nanocomposites. *Mater Sci Eng C* 28:1–10
- Ray SS, Bousmina M (2005) Biodegradable polymers and their layered silicate nanocomposites: in greening the 21st century materials world. *Prog Mater Sci* 50:962–1079
- Solarski S, Ferreira M, Devaux E (2008) Ageing of polylactide and polylactide nanocomposite filaments. *Polym Degrad Stab* 93:707–712
- Hiroi R, Ray SS, Okamoto M, Shiroi T (2004) Organically modified layered titanate: a new nanofiller to improve the performance of biodegradable polylactide. *Macromol Rapid Commun* 25: 1359–1364
- Nam JY, Ray SS, Okamoto M (2003) Crystallization behavior and morphology of biodegradable polylactide/layered silicate nanocomposite. *Macromolecules* 36:7126–7131
- Xiao YM, Li DX, Fan HS, Li XD, Gu ZW, Zhang XD (2007) Preparation of nano-HA/PLA composite by modified-PLA for controlling the growth of HA crystals. *Mater Lett* 61:59–62
- Russias J, Saiz E, Nalla RK, Gryn K, Ritchie RO, Tomsia AP (2006) Fabrication and mechanical properties of PLA/HA composites: a study of in vitro degradation. *Mater Sci Eng C* 26:1289–1295
- Xu XL, Chen XS, Liu AX, Hong ZK, Jing XB (2007) Electrospun poly(L-lactide)-grafted hydroxyapatite/poly(L-lactide) nanocomposite fibers. *Eur Polym J* 43:3187–3196
- Goffin AL, Duquesne E, Moins S, Alexandre M, Dubois P (2007) New organic-inorganic nanohybrids via ring opening polymerization of (di)lactones initiated by functionalized polyhedral oligomeric silsesquioxane. *Eur Polym J* 43:4103–4113
- Pan H, Qiu Z (2010) Biodegradable Poly(L-lactide)/polyhedral oligomeric silsesquioxanes nanocomposites: enhanced crystallization, mechanical properties, and hydrolytic degradation. *Macromolecules* 43:1499–1506
- Wu CS, Liao HT (2007) Study on the preparation and characterization of biodegradable polylactide/multi-walled carbon nanotubes nanocomposites. *Polymer* 48:4449–4458
- Song WH, Zheng Z, Tang WL, Wang XL (2007) A facile approach to covalently functionalized carbon nanotubes with biocompatible polymer. *Polymer* 48:3658–3663
- Xu JZ, Chen T, Yang CL, Li ZM, Mao YM, Zeng BQ, Hsiao BS (2010) Isothermal crystallization of poly(L-lactide) induced by graphene nanosheets and carbon nanotubes: a comparative study. *Macromolecules* 43:5000–5008
- Murariu M, Dechief AL, Bonnaud L, Paint Y, Gallos A, Fontaine G, Bourbigot S, Dubois P (2010) The production and properties of polylactide composites filled with expanded graphite. *Polym Degrad Stab* 95:889–900
- Kim I-H, Jeong YG (2010) Polylactide/exfoliated graphite nanocomposites with enhanced thermal stability, mechanical modulus, and electrical conductivity. *J Polym Sci B* 48:850–858
- Cao Y, Feng J, Wu P (2010) Preparation of organically dispersible graphene nanosheet powders through a lyophilization method and their poly(lactic acid) composites. *Carbon* 48:3834–3839
- Hussain F, Hojjati M, Okamoto M, Gorga RE (2006) Polymer-matrix nanocomposites, processing, manufacturing, and application: an overview. *J Compos Mater* 40:1511–1575
- Chung DDL (2002) Review graphite. *J Mater Sci* 37:1475–1489
- Potts JR, Dreyer DR, Bielawski CW, Ruoff RS (2011) Graphene-based polymer nanocomposites. *Polymer* 52:5–25
- Zhao YF, Xiao M, Wang SJ, Ge XC, Meng YZ (2007) Preparation and properties of electrically conductive PPS/expanded graphite nanocomposites. *Compos Sci Technol* 67:2528–2534
- Uhl FM, Yao Q, Nakajima H, Manias E, Wilkie CA (2005) Expandable graphite/polyamide-6 nanocomposites. *Polym Degrad Stab* 89:70–84
- Yasmin A, Luo JJ, Daniel IM (2006) Processing of expanded graphite reinforced polymer nanocomposites. *Compos Sci Technol* 66:1182–1189
- Chen G, Weng W, Wu D, Wu C (2003) PMMA/graphite nanosheets composite and its conducting properties. *Eur Polym J* 39:2329–2335

38. Kalaitzidou K, Fukushima H, Drza LT (2007) A new compounding method for exfoliated graphite–polypropylene nanocomposites with enhanced flexural properties and lower percolation threshold. *Compos Sci Technol* 67:2045–2051
39. Chen G, Chen X, Wang H, Wu D (2007) Dispersion of graphite nanosheets in polymer resins via masterbatch technique. *J Appl Polym Sci* 103:3470–3475
40. Deshmukh K, Khatake SM, Joshi GM (2013) Surface properties of graphene oxide reinforced polyvinyl chloride nanocomposites. *J Polym Res* 20:286
41. Park S, Ruoff RS (2009) Chemical methods for the production of graphenes. *Nat Nanotechnol* 4:217–224
42. Paredes JJ, Villar-Rodil S, Martinez-Alonso A, Tascon JM (2008) Graphene oxide dispersions in organic solvents. *Langmuir* 24:10560–10564
43. Dreyer DR, Park S, Bielawski CW, Ruoff RS (2010) The chemistry of graphene oxide. *Chem Soc Rev* 39:228–240
44. Bourlinos AB, Gournis, Petridis D, Szabo T, Szeri A, Dekany I (2003) Graphite oxide: chemical reduction to graphite and surface modification with primary aliphatic amines and amino acids. *Langmuir* 19:6050–6055
45. Li W, Tang XZ, Zhang HB, Jiang ZG, Yu ZZ, Du XS, Mai YW (2011) Simultaneous surface functionalization and reduction of graphene oxide with octadecylamine for electrically conductive polystyrene composites. *Carbon* 49:4724–4730
46. Cao Y, Feng J, Wu P (2010) Alkyl-functionalized graphene nanosheets with improved lipophilicity. *Carbon* 48:1683–1685
47. Niyogi S, Bekyarova E, Itkis ME, McWilliams JL, Hamon MA, Haddon RC (2006) *J Am Chem Soc* 128:7720
48. Bai S, Shen X, Zhu G, Xu Z, Liu Y (2011) Reversible phase transfer of graphene oxide and its use in the synthesis of graphene-based hybrid materials. *Carbon* 49:4563–4570
49. Wang G, Shen X, Wang B, Yao J, Park J (2009) Synthesis and characterisation of hydrophilic and organophilic graphene nanosheets. *Carbon* 47:1359–1364
50. Park HM, Liang X, Mohanty AK, Misra M, Drzal LT (2004) Effect of compatibilizer on nanostructure of the biodegradable cellulose acetate/organoclay nanocomposites. *Macromolecules* 37:9076–9082
51. Wang Y, Tsai HB (2012) Thermal, dynamic-mechanical, and dielectric properties of surfactant intercalated graphite oxide filled maleated polypropylene nanocomposites. *J App Polym Sci* 123:3154–3163
52. Mishra JK, Hwang KJ, Ha CS (2005) Preparation, mechanical and rheological properties of a thermoplastic polyolefin (TPO)/organoclay nanocomposite with reference to the effect of maleic anhydride modified polypropylene as a compatibilizer. *Polymer* 46:1995–2002
53. Petersson L, Oksman K, Mathew AP (2006) Using maleic anhydride grafted poly(lactic acid) as a compatibilizer in poly(lactic acid)/layered-silicate nanocomposites. *J Appl Polym Sci* 102:1852–1862
54. Zhang JF, Sun X (2004) Mechanical properties of poly(lactic acid)/starch composites compatibilized by maleic anhydride. *Biomacromolecules* 5:1446–1451
55. Yuan H, Liu Z, Ren J (2009) Preparation, characterization, and foaming behavior of poly(lactic acid)/poly(butylene adipate-co-butylene terephthalate) blend. *Polym Eng Sci* 49:1004–1012
56. Hummers WS, Offeman RE (1958) Preparation of graphitic oxide. *J Am Chem Soc* 80:1339–39
57. Matsuo T, Niwa T, Sugie Y (1999) Preparation and characterization of cationic surfactant-intercalated graphite oxide. *Carbon* 37:897–901
58. Nethravathi C, Rajamathi M (2006) Delamination, colloidal dispersion and reassembly of alkylamine intercalated graphite oxide in alcohols. *Carbon* 44:2635–2641
59. Kalaitzidou K, Fukushima H, Drzal LT (2007) Multifunctional polypropylene composites produced by incorporation of exfoliated graphite nanoplatelets. *Carbon* 45:1446–1452
60. Schniepp HC, Li JL, McAllister MJ, Sai H, Herrera-Alonso M, Adamson DH, Prud'homme RK, Car R, Saville DA, Aksay IA (2006) Functionalized single graphene sheets derived from splitting graphite oxide. *J Phys Chem B* 110:8535–8539
61. Meyer JC, Geim AK, Katsnelson MI, Novoselov KS, Booth TJ, Roth S (2007) The structure of suspended graphene sheets. *Nature* 446:60–63
62. Zhang S, Xiong P, Yang X, Wang X (2011) Novel PEG functionalized graphene nanosheets: enhancement of dispersibility and thermal stability. *Nanoscale* 3:2169–2174
63. Lonkar SP, Therias S, Leroux F, Gardette JL, Singh RP (2011) Influence of reactive compatibilization on the structure and properties of PP/LDH nanocomposites. *Polym Inter* 60:1688–1696
64. Wang H, Qiu Z (2012) Crystallization kinetics and morphology of biodegradable poly(l-lactic acid)/graphene oxide nanocomposites: Influences of graphene oxide loading and crystallization temperature. *Thermochim Acta* 527:40–46
65. Zheng W, Wong SC (2003) Electrical conductivity and dielectric properties of PMMA/expanded graphite composites. *Compos Sci Technol* 63:225–235
66. Starkweather HW, Avakian P (1992) Conductivity and the electric modulus in polymers. *J Polym Sci B Polym Phys* 30:637–641